Mansoura Engineering Journal

Volume 27 | Issue 3 Article 5

1-24-2021

Measurements of Heat Transfer and Fluid Flow in a Rectangular Duct with Different Types of Rib-Turbulators.

K. Morad
Mechanical Power Department., Faculty of Engineering., Suez Canal University., Port Said., Egypt.

I. El-Sawaf
Mechanical Power Dept., Faculty of Engineering., Suez Canal University., Port Said., Egypt.

MEASUREMENTS OF HEAT TRANSFER AND FLUID FLOW IN A RECTANGULAR DUCT WITH DIFFERENT TYPES OF RIB-TURBULATORS

K.A. Morad and I.A. El-Sawaf
Mechanical Power Dept., Faculty of Engineering
Suez Canal University, Prot Said, Egypt.

قياسات لإنتقال الحراره وتدفق المائع فى قناه مستطيله مع أنواع مختلفه من العروق المسببه للدواميه

خلاصه

فى هذا البحث أجريت التجارب المعمليه لدراسة إنتقال الحراره وفواقد الإحتكاك خلال قناه ذات مقطع مستطيل خشنت أرضيتها بصفوف من العروق مختلفة الأشكال (عروق ذات مقطع مربع ومثلثى ودائرى). وتراوح رقم رينولدز المعتمد على القطر الهيدروليكى لقناة الإختبار مابين ١٢٠٠٠ إلى ٦٠٠٠٠ بينما تراوحت النسبه بين خطوة العرق (المسافه بين عرقين متتاليين) وإرتفاعه مابين ٦ إلى ١٨. ولفهم آلية زيادة معدل إنتقال الحراره بتخشين السطح بإستخدام العروق قيست أيضا السرعات المتوسطه للمائع المتدفق فى حالة القناه المخشنه بواسطة العروق المربعه.

نتائج البحث توضح بأن الهواء المتدفق خلال القناه المخشنه بواسطة العروق يصبح كامل التدفق دوريا بعد العرق الثالث من مدخل القناه ذات العروق، وتوضح نتائج البحث أيضا بأن العروق ذات الشكل المثلثى تنتج أعلى زياده فى معدل إنتقال الحراره من الأنواع الأخرى المستخدمه فى هذا البحث. كما توضح النتائج أيضا بأن نسبة الزياده فى معدل إنتقال الحراره (التى تتمثل فى النسبه بين رقم نوسلت للقناة المخشنه إلى رقم نوسلت للقناة الغير مخشنه) تكون أكبر من نسبة الزياده فى فواقد الضغط (التى تتمثل فى النسبه بين معامل الإحتكاك للقناة المخشنه الى معامل الإحتكاك للقناة الغير مخشنه) المرتبطه بإستخدام العروق فى الأنفاق المستطيله. ومن دراسة تأثير معامل التوصيل الحرارى لمادة العروق المستخدمه يتضح بأن التوصيل الحرارى لمادة العروق يؤثر تأثير ملحوظ على الزياده فى معدل انتقال الحراره (يزداد بزيادة معامل التوصيل الحرارى لمادة العرق). وقد تم فى هذا البحث إستنباط علاقات متبادله تربط كلا من الزياده فى معدل إنتقال الحراره وفواقد الإحتكاك المرتبطه بإستخدام العروق ذات المقطع المربع فى القنوات المستطيله بكلا من رقم رينولدز والنسبه بين خطوة العرق وإرتفاعه.

ABSTRACT

Experiments are conducted to study the heat transfer and friction in a rectangular duct roughened by arrays of alternate ribs (square-, triangle-, and circle-shaped ribs). The Reynolds number *Re* based on duct hydraulic diameter rages from *12.000* to *60.000*, whereas the rib pitch-to-height ratio (*P/h*) varies from *6* to *18*. To understand the mechanism of heat transfer enhancement the measurements of streamwise mean velocities are also conducted in the square-ribbed duct. The results show that the flow of air through the ribbed duct becomes periodically fully developed after the third rib from the duct inlet. The data indicate also that the triangular type ribs have a substantially higher heat transfer performance than any other ribs in the studied range. The experimental results show that the heat transfer enhancement factors are greater than the friction factor ratios associated with the use of rib-turbulators in the rectangular ducts. Also, the rib conductivity affects significantly on the heat transfer enhancement factor. Correlations for friction and heat transfer in square-ribbed ducts are developed to account for rib spacing to height ratio and flow Reynolds number.

Keywords: Heat transfer enhancement, Friction factor; Rib-turbulator; Ribbed duct; Rib-shaped geometries; Rib thermal conductivity; Constant heat flux.

Accepted August 26, 2002.

Nomenclature

A_P	heat transfer surface area of the ribbed duct, m^2
D_h	hydraulic diameter, $D_h = 2WH/(W+H)$, m
f	friction factor
f_P	friction factor for the ribbed duct
f_s	friction factor for the smooth duct
h	rib height, m
H	height of the duct, m
k_a	air thermal conductivity, $W/m\ K$
k_w	wood thermal conductivity, $W/m\ K$
Nu_x	local Nusselt number
Nu_P	average Nusselt number for the periodically fully developed ribbed duct flow
Nu_s	average Nusselt number for the smooth duct flow
P	rib pitch, m
Pr	Prandtl number
Δp	pressure drop through the periodically fully developed duct flow, Pa
$\dot{Q}_c$	net heat transfer rate, W
Re	Reynolds number, $U_\infty D_h/\nu$
T_b	local bulk temperature of air, K
T_w	local wall temperature, K
U_∞	free stream velocity, m/s
u	streamwise mean velocity at different y-positions, m/s
W	width of the duct, m
x	axial coordinate ($x = 0$ at the upstream edge of test plate)
$X_{N,r}$	position of reattachment point downstream of the rib
y	transverse coordinate, see ***Fig. 3***

Subscripts

b	bulk
N	rib index
s	smooth
w	wall
con	conduction
P	periodically
rad	radiation

Greek Symbol

ρ air density, kg/m^3

ν air kinematic viscosity, m^2/s

1. INTRODUCTION

A well-known method to increase the heat transfer is to roughen the surface either with a sand grain or by use of regular geometric roughness elements (fins or ribs) on the surface. However, the increase in heat transfer is accompanied by an increase in the resistance to fluid flow. Many investigators have studied this problem in an attempt to develop accurate predictions of the behavior of a given roughness geometry and to define a geometry which gives the best heat transfer performance.

Fluid flow associated with heat transfer in a fin-array duct or ribbed duct has been a subject of extensive research in the past two decades because of its significance in a wide variety of practical applications, for example, turbine blade cooling and heat exchangers. Hwang and Lui [1] conducted an experimental study to compare the overall heat transfer coefficients in straight and 90^o turned trapezoidal ducts with pin-

fin arrays. The optimum shape and arrangement of staggered pins in a rectangular channel to give the optimization between the pressure drop and heat transfer were studied by Lee et al. [2].

Many experimental and numerical works were carried out to investigate the heat transfer characteristics of rib-roughened surface. Webb et al. [3] presented heat transfer and pressure drop data for fully developed turbulent flow in circular tubes with transverse square ribs attached internally. Gee and Web [4] studied experimentally the effect of the rib helix angle on turbulent heat transfer and friction loss for fully developed flow in circular tubes, the helical rib roughness yields greater heat transfer per unit friction than the transverse rib roughness with the preferred helix angle approximately 49^{o}. Sparrow and Tao [5] investigated the effects of the Reynolds number ($10,000 \leq Re \leq 45,000$) and the rib pitch to height ratio ($P/h = 9.15$, 18.3, and 36.6) on the mass transfer coefficient and the friction factor for developing duct flows with rod ribs attached both on two opposite walls and on one wall only of a rectangular duct. The mass transfer was determined by using the naphthalene sublimation technique, but metallic rib-turbulators were not coated with naphthalene, and therefore, the contribution of additional surface area due to the presence of circular rods to heat transfer enhancement was not considered. Hwang [6] investigated a comparison of fully developed heat transfer characteristics in rectangular ducts with one wall roughened by slit and solid ribs. He concluded that the slit-ribbed geometry gives higher ribbed-channel heat transfer than the solid-ribbed geometry. The flow characteristics in a rectangular channel downstream of a backward facing step and four rib-turbulator arrangements were compared by Roclawski et al. [7]. They found that the flow through the ribbed channel could be characterized by a series of accelerations, decelerations with separation, reattachment and redevelopment due to the sudden changes in cross-section.

Numerical investigations concerned with heat transfer and pressure drop characteristics in a ribbed duct have become available recently, such as the studies by Tsai et al. [8], Bredberg and Davidson [9], Kwang Kim and Sun Kim [10], and Bredberg et al. [11]. The turbulence models used in these studies were a k-ε model, k-ω model, and an explicit algebraic Reynolds stress model.

The main objective of the present study is to investigate the effects of rib shapes on the heat transfer and friction in rectangular channels. Measurements of different rib shapes: square-, circle-, and triangle-shaped geometries are made. Moreover, two components that contribute to the heat transfer enhancement, i.e., additional heat transfer surface area, and improved turbulent mixing, are intentionally separated by examining the effect of rib conductivity on the heat transfer. Centerline local heat transfer coefficient distribution and average heat transfer coefficient and friction factor in the periodically fully developed regime are measured on the bottom-ribbed wall of the test channel. The geometric parameter was varied within the range of $6 \leq P/h \leq 18$. The distribution of mean streamwise velocity component at different axial positions is also investigated for the assistance of understanding the mechanism of heat transfer enhancement. Correlations for the friction factor and average Nusselt, Nu_{ρ}, number for fully developed turbulent flow in rectangular channel with repeated square rib-roughness are successfully developed in terms of Re number and geometry parameter P/h.

2. EXPERIMENTAL SETUP AND DATA REDUCTION

2.1 Experimental Setup

Figure 1 shows the airflow system and experimental apparatus employed. A centrifugal blower forced air through the test section. The major components of the experimental setup have been previously described by Morad [12].

The test duct is *300 mm* long, with a rectangular cross section of *220 mm* (width, *W*) by *120 mm* (height, *H*) for a duct aspect ratio (*W/H*) of *1.83*. The bottom wall serves as a heat transfer surface roughened by a series of ribs, while the top and two vertical walls are smooth. The rib spans the entire width of the test section. Aluminum bars of square cross-section (*5* by *5 mm*), circular cross-section (*5 mm* in diameter), or triangular cross-section (*5 mm* base and height) are attached to the heated wall alternately. The ribs are glued uniformly on the heated surface by thermal epoxy. In the baseline experiments (square rib with *P/h = 6*), the ribbed wall is arranged: three thermocouples within every rib pitch, which are located at *1.5, 3, 4.5h* downstream of rib rear face, respectively. In addition, the top wall of each rib has one thermocouple. These thermocouples embedded flush on the top wall of the ribs to avoid flow disturbance. All thermocouples are copper-constantan thermocouples of *0.25 mm* in diameter. The rear face of the first rib located at a distance of one pitch from the upstream edge of the heated surface. At different axial positions, a thermocouple probe inserted from the top duct wall into the duct flow to measure the bulk air temperature. The pressure drop measurements were performed using an aluminum test plate under isothermal condition; i.e., without heat flux. Two pressure taps are connected to an inclined manometer to measure the pressure drop across the periodically fully developed flow. The mean streamwise velocity distribution at different axial positions are measured by a spherical *5-hole* probe with a sphere diameter of *2.9* mm and pressure tap diameters of *0.3 mm* [12&16].

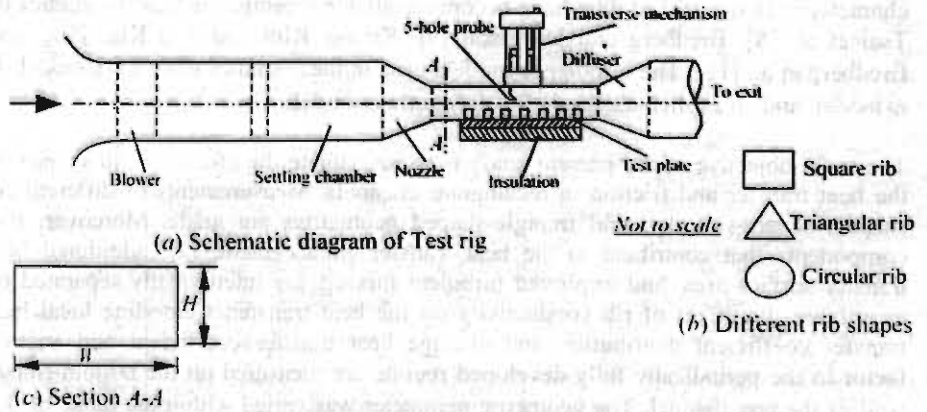

(*a*) Schematic diagram of Test rig

(*b*) Different rib shapes

(*c*) Section *A-A*

Fig. 1: Schematic diagram of experimental setup

The heat transfer test surface is a constant heat flux flat plate surface (***Fig. 2***). It consists of a number of stainless steel strips placed side-by-side and glued to a *PVC*-plate using *0.13 mm* thick adhesive polymer film. The *PVC*-plate not only forms the structural portion of the surface, but also reduces the heat losses by conduction. The

Styrofoam insulation behind the plate is approximately *50 mm* thick. The stainless steel heaters are *0.5 mm* thick by *20 mm* in the flow direction and spaced *0.2 mm* apart (*Fig. 2*). The heater strips were sprayed with a coating material (Nextel Valvet Coating) of emissivity $\varepsilon = 0.95$. The individual metal strips are connected in series by heavy stainless steel bus bars. To prevent the electrical contact between the bus bars and the sidewalls of the test section, the bus bars were covered with a sheet of *PVC*. Thermocouples, of diameter *0.25 mm*, are bonded in special grooves in the *PVC* base plate beneath the foil strips. They are used to measure the surface temperature distribution. The thermocouple leads run in opposite directions along the surface for a short distance to minimize heat loss through them. Thermocouples are also attached to the back of the *PVC* plate at various locations in order to determine that portion of heat dissipated in the strips which is conducted through the *PVC* plate. Power for the heaters is provided by *900 Watt DC* power supply wired in series with the heaters and with a reference resistance (*5 mΩ*). Current flow is determined from the voltage drop across the reference resistance and the heat generated is calculated from the current flow and the voltage drop across the heaters.

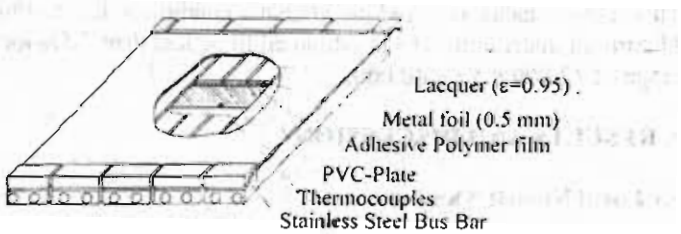

Fig. 2: Schematic diagram of constant heat flux test plate.

2.2 Data Reduction

The local convection heat transfer coefficient of the heated surface is correlated in terms of the local *Nu* number, which is defined as

$$Nu = \frac{\dot{Q}_c D_h}{A_p (T_w - T_b) k_a} \qquad (1)$$

where D_h is the hydraulic diameter ($D_h = 2WH/(W+H)$). Here, $\dot{Q}_c$ is the net heat transfer rate from the ribbed wall to the air, and is calculated by subtracting the heat losses (conduction and radiation losses) from the supplied electrical power. The electrical power generated from the foil strips is determined from the measured current flow and the voltage drop across the foil strips. The total heat losses, during the experiments is estimated by:

$$\dot{Q}_l = \dot{Q}_{cond} + \dot{Q}_{rad} \qquad (2)$$

$\dot{Q}_{cond}$ is the conductive heat loss, which was calculated by assuming one-dimensional heat conduction through the test plate as in Morad [12]. Radiation heat loss, $\dot{Q}_{rad}$, can be calculated by estimating the radiation configuration factors between the heated surface ($\varepsilon = 0.95$) and other walls of the test section. The approximate magnitudes of

heat losses were as follows: radiation, *13%* and conduction, *2.5%* of the electrical heat generation.

In ***Eq.*** (1), T_b is the bulk temperature of air measured using a thermocouple probe. The inlet bulk air temperature is *25-28°C* depending on the test condition. The projected surface area of the corresponding ribless wall serves as the heat transfer surface area (A_p) in ***Eq.*** (*1*). By using the estimation method of Kline and McClintock [13], the maximum uncertainty of *Nu* number is less than *8.2%* for the *Re* number range of $12{,}000 \le Re \le 60{,}000$. The fully developed average Nusselt number, Nu_P, is determined by averaging the local *Nu* numbers through the periodically fully developed region.

In fully developed duct flow with mean free stream velocity of air, U_∞, the Fanning friction factor [17] was calculated from the static pressure drop across the periodically fully developed region as:

$$f = \frac{\Delta p}{\rho U_\infty^2 / 2}\left(\frac{D_h}{4P}\right) \qquad [17] \qquad (3)$$

This friction factor is based on adiabatic conditions, i.e., testing without wall heating. Maximum uncertainty of f is estimated to be less than *7.5%* for the case of *Re* number range of $12{,}000 \le Re \le 60{,}000$.

3. RESULTS AND DISCUSSION

3.1 Local Nusselt Number

Figure 4 shows the local *Nu* number distribution along the axial distance of the ribbed wall with $Re = 12{,}000$. In this figure, the local *Nu* number is plotted as a function of the dimensionless coordinate *x/h*. The rib pitch to height ratio (*P/h*) is fixed at value of *6*. The local *Nu* number along the axial distance starts with a local maximum value at the immediate region of ribbed-wall inlet, the local *Nu* number decreases along the axial distance. Two maximum values of *Nu* occur at the top of each rib ($x/h \approx 6.5, 12.5, 18.5$, *etc.*) and at the reattachment point of the separated flow ($x/h \approx 10, 16, 22$, etc.), respectively, and two minimum values occur at the separation regions immediately upstream and downstream of each rib as shown in ***Fig. 3***, which shows the conceptual view of the flow patterns around the rib-roughened wall. The position of reattachment point, $X_{X,r}$, is approximately *3h* downstream of each rib. The *Nu* number distribution approaches a periodic fully developed distribution after the third rib of the ribbed wall, where the distribution of local *Nu* number becomes approximately the same for each rib pitch after $x/h = 24$ ($N = 3$), as shown in ***Fig. 4***.

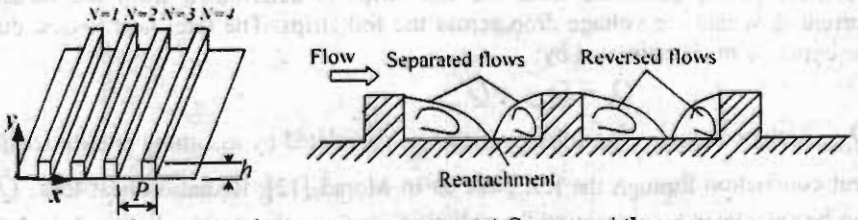

(*b*) Orientation of x- and y-axis (*a*) Conceptual flow pattern

Fig. 3: Square-ribbed wall investigated

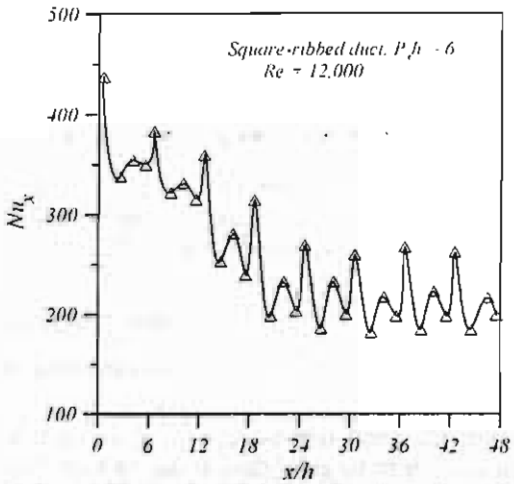

Fig. 4: Local *Nu* number distributions along the axial distance.

3.2 Mean Streamwise Velocity

To confirm the above hypothesis, streamwise mean velocity in the region downstream of four ribs (from $N = 1$ to $N = 4$, where N is the rib index) are obtained with a *5-hole* probe measurements in the cold flow condition. The probe insertion location is at a distance of four rib-heights from each rib rear face (i.e., $x_N = 4h$), where it is believed to be out of the flow separation ($X_{N,r} \approx 3$). Measured distribution of mean velocity ratio, u/U_∞, is shown in ***Fig. 5***, where U_∞ denotes the free stream velocity. It is observed that the distribution u/U_∞ changes significantly after the first rib to that after the second rib. The distribution of u/U_∞ appears to be the same after the third and after the fourth ribs, as shown in ***Fig. 5***. This means that the flow becomes periodically fully developed after the third rib.

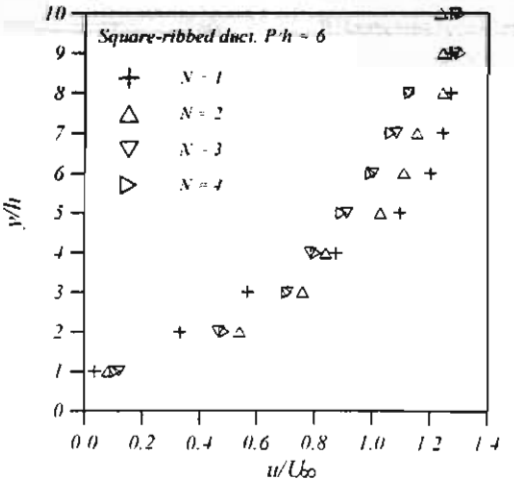

Fig. 5: Streamwise mean velocities at several axial positions.

3.3 Periodically Fully Developed Flow Results

3.3.1 Effects of Rib Type

Prior to ribbed duct experiments for friction factors and heat transfer for roughened-ribbed wall, fully developed friction factors and heat transfer coefficients are measured for a smooth duct and compared with results given in the literature, as shown in ***Figs.*** *6* and *7*. The correlations for comparison includes Blasius equation for friction and Dittus-Boelter equation for heat transfer [14]:

$$f_s = 0.079\,\mathrm{Re}^{-0.25} \qquad \text{Blasius correlation [14]} \qquad (4)$$

$$Nu_s = 0.023\,\mathrm{Re}^{0.2}\,\mathrm{Pr}^{0.8} \qquad \text{Dittus-Boelter correlation [14]} \qquad (5)$$

The two equations provide good representations of the data for fully developed turbulent gas flow in smooth rectangular duct. It can be seen from these figures that the present fully developed *Nu* number and friction factors for smooth tube compared well with the previous correlations. A fairly satisfactory agreement in the above comparison has confirmed that the experimental procedure employed is adequate and the results obtained are reliable. *Figure 6* shows the friction factors for different rib types shown previously in ***Fig.*** *1(b)* for the same ribbed height and spacing (*P/h* = *6*). The square-shaped geometry has the highest value of friction factors because of its stronger turbulence mixing caused by the ribs. ***Figure*** *7* indicates that the Nu_P numbers of the triangle- and square-shaped ribs are much higher than the circle-shaped geometry. It is probably because the turbulence mixing becomes more significant in the sharp square- and triangle-shaped geometries. Close inspection of this figure further shows that, it being different from that in ***Fig.*** *6*, as the heat transfer for triangle-shaped ribs is highest.

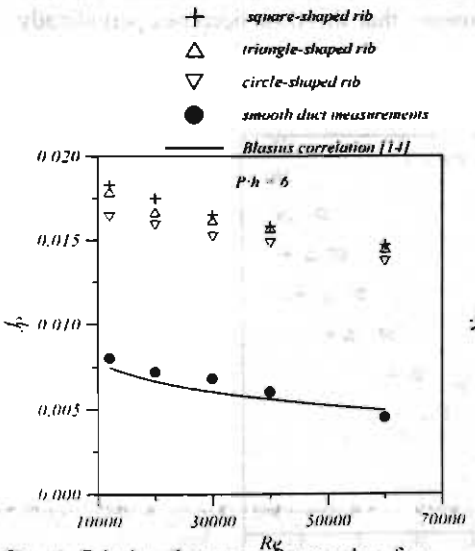

Fig. *6*: Friction factor vs *Re* number for different rib types.

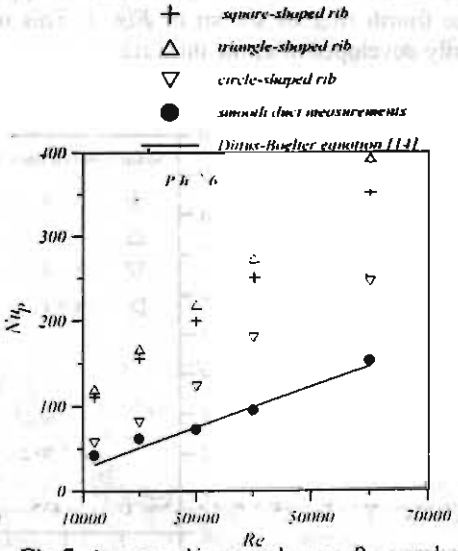

Fig. *7*: Average Nu_P number vs *Re* number for different rib types.

Figures 8 and *9*, respectively, show the heat transfer enhancement factors and friction factor ratios for the three types of ribs investigated as a function of *Re* number. The heat transfer enhancement factor is calculated by normalizing the average Nu_P number for the ribbed wall duct by the average Nu_s number for smooth duct given by ***Eq.*** *(5)*. Also, the ribbed wall friction factors are normalized by the friction factors for fully developed flow in smooth duct calculated by ***Eq.*** *(4)* to give the friction factor ratios, f_P/f_s. The enhancement factor decreases continuously with increasing *Re* number for square- and triangle-shaped geometries but the triangle-shaped ribs give the highest enhancement factors, Nu_P/Nu_s, as shown in ***Fig.*** *8*. The optimum enhancement factor for circle-shaped rib occurs at approximately *Re = 40,000*. ***Figure*** *9* shows that the friction factor ratios, f_P/f_s, for triangle-shaped ribs are lower than for square-shaped ribs and the minimum values of f_P/f_s are for circle-shaped geometry.

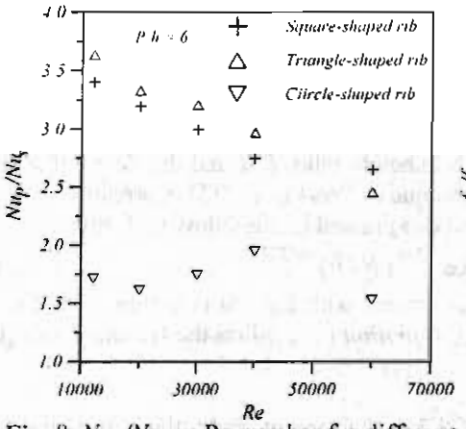

Fig. *8*: Nu_P/Nu_s vs Re number for different rib types.

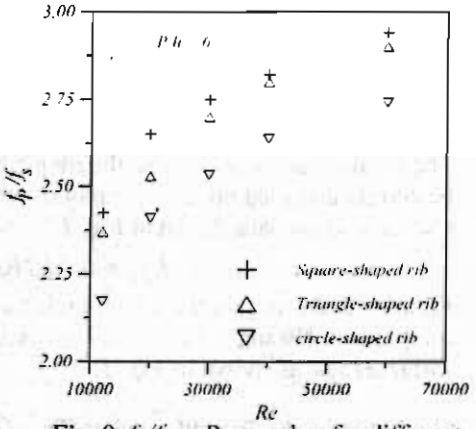

Fig. *9*: f_P/f_s vs Re number for different rib types.

3.3.2 Effects of Rib Pitch to Height Ratio

Figures *10* and *11*, respectively, show the heat transfer enhancement factor and friction factor ratio for periodically fully developed flow in a ribbed-wall channel with square-shaped geometry as a function of Re number for different rib pitch to height ratios (*P/h = 6, 12,* and *18*). Heat transfer enhancement factors and friction factor ratios are roughly between *3.4 – 1.8* and *3 - 1.5*, respectively, times that of the fully developed smooth duct. For different values of *P/h*, the enhancement factor decreases and the friction factor ratio increases with increasing Reynolds number, as shown in ***Figs.*** *10* and *11*. As observed from these figures, the heat transfer enhancement factor and friction factor ratio decrease with increasing rib pitch to height ratio because of less frequency of duct blockages. It is important to mention that the average *Nu* numbers presented are based on the smooth wall surface area for the three values of *P/h* investigated. Consequently, the magnitudes of the average *Nu* number obtained by the present work reflects the combined two augmented factors, i.e., the enhanced turbulence mixing by distorting the flow fields caused by the presence of ribs, and the extension in heat transfer surfaces (fin effect) provided by ribs.

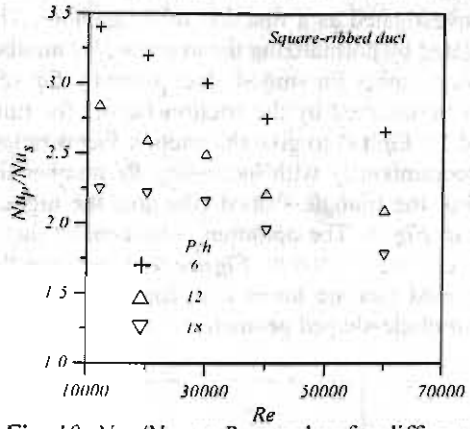

Fig. 10: Nu_P/Nu_s vs *Re* number for different rib pitch to height ratio, *P/h*.

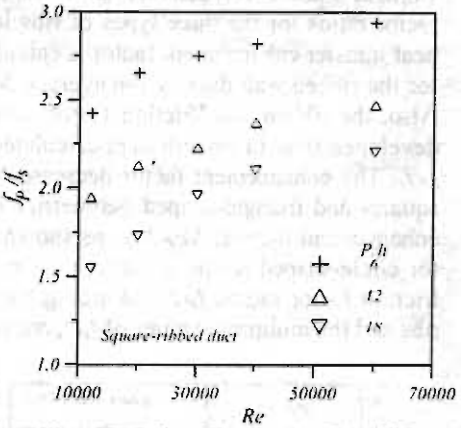

Fig. 11: f_P/f_s vs *Re* number for different rib pitch to height ratio, *P/h*.

The friction factor ratio, f_P/fs, the rib pitch to height ratio. *P/h*. and the *Re* number can be correlated based on the asymptotic technique of Press et al. [15]. Correlation of the present friction data shown in ***Fig.*** *11* can be expressed in the following form:

$$f_P / f_s = 0.518\,\mathrm{Re}^{0.228}(P/h)^{-0.372} \qquad (6)$$

Figure *12* shows that the uncertainties associated with ***Eq.*** *(6)* is within *10%*. For a comparison, Hwang's data [6] is involved. ***Equation*** (6) predicts the Hwang's data [6] within *±15%*, as shown in ***Fig.*** *12*.

Similarly, for the Prandtl number, *Pr*, of *0.7* in the present study, the correlation for the heat transfer enhancement factors shown in ***Fig.*** *10* can be represented by:

$$Nu_P / Nu_s = 34.976\,\mathrm{Re}^{-0.180}(P/h)^{-0.339} \qquad (7)$$

Figure *13* shows that the uncertainties associated with ***Eq.*** (7) is within *±7%*. As shown in this figure, again, the present correlation predicted well the Hwang's data [6] within *±11%*.

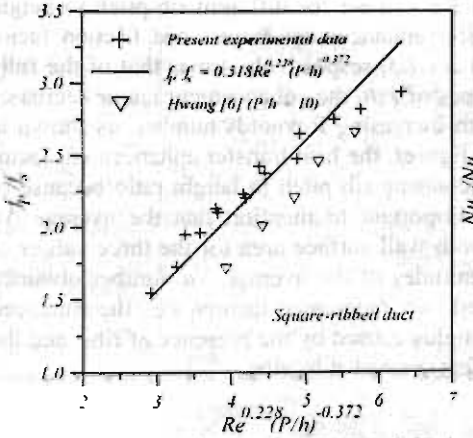

Fig. 12: f_P/f_s correlation for square-ribbed duct.

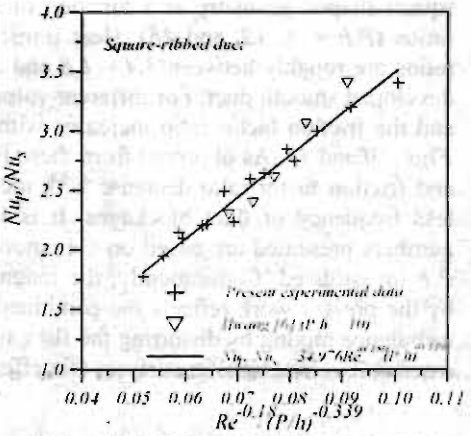

Fig. 13: Nu_P/Nu_s correlation for square-ribbed duct.

3.3.3 Effect of Rib Conductivity

It is very instructive to separate the above-mentioned two components that contribute to heat transfer enhancement of the rib-roughened wall, i.e., increase in turbulence mixing, and extension in heat transfer surface area. For this purpose, the effect of the rib conductivity on the heat transfer enhancement factor for periodically fully developed flow is examined and shown in ***Fig. 14***. In this study, wood ribs (k_w = *0.1 W/m K*) instead of aluminum ribs serves as thermally-nonactive turbulators. The duct with thermally-nonactive ribs provides the worse heat transfer enhancement factors. An important conclusion is drawn from this figure, for the ribbed wall, the thermally active rib has a higher heat transfer enhancement factors than the thermally-nonactive rib. This implies that the rib conduction (or increase in surface area) has contributed significantly to heat transfer enhancement for rib-roughened wall.

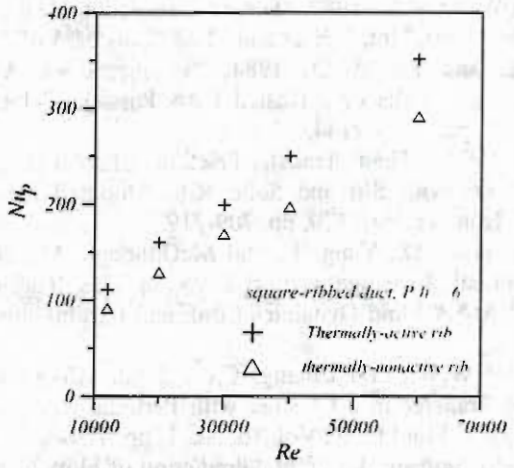

Fig. 14: effect of rib conductivity on the average Nu_p number for periodically fully developed square-ribbed duct

4. SUMMARY AND CONCLUSIONS

The effects of rib shape, rib pitch to height ratio, and rib thermal conductivity, on heat transfer and pressure losses in rectangular duct have been examined experimentally. The main findings from the experiments are as follows:

1- The flow approaches a periodically fully developed regime after the third rib from the duct inlet.
2- Heat transfer enhancement factor decreases and friction factor ratio increases with increasing *Re* number for square- and triangle-shaped ribs.
3- The square-shaped ribs have the highest value of friction factor, while the triangle-shaped ribs have the highest value of heat transfer enhancement factor.
4- The heat transfer enhancement factors are greater than the friction factor ratios associated with the use of rib-turbulators in the rectangular ducts.
5- Heat transfer enhancement factor and friction factor ratio decreases with increasing rib pitch to height ratio because of less frequently of duct blockages.

6- The rib conductivity affects significantly the heat transfer enhancement factor, which increases with increasing rib conductivity.

5. REFERENCES

[1] Hwang, J.J., and Lui, C.C., 1999, "Detailed Heat Transfer Characteristic Comparison in Straight and 90-Deg Turned Trapezoidal Ducts with Pin-Fin Arrays." Int. J. Heat and Mass Transfer, Vol. 42, pp. 4005-4016.

[2] Lee, K.S., Kim, W.S., and Si, J.M., 2001, "Optimal Shape and Arrangement of Staggered Pins in the Channel of a Plate Heat Exchanger." Int. J. Heat and Mass Transfer, Vol. 44, pp. 3223-3231.

[3] Webb, R.L., Eckert, R.J., and Goldstein, R.J., 1971, "Heat Transfer and Friction in Tubes with Repeated Rib Roughness," Int. J. Heat and Mass Transfer, Vol. 14, pp. 601-617.

[4] Gee, D.L., and Webb, R.L., 1980, "Forced Convection Heat Transfer in Helically Rib-Roughened Tubes," Int. J. Heat and Mass Transfer, Vol. 23, pp. 1127-1136.

[5] Sparrow, E.M., and Tao, W.Q., 1984, "Symmetric vs. Asymmetric Periodic Disturbances at the Walls of a Heated Flow Passages." Int. J. Heat and Mass Transfer, Vol. 27, pp. 2133-2144.

[6] Hwang, J.J., 1998, "Heat Transfer-Friction Characteristics Comparison in Rectangular Ducts with Slit and Solid Ribs Mounted on one Wall." ASME Trans., J. Heat Transfer, Vol. 120, pp. 709-719.

[7] Roclawski, H., Jacob, D., Yang, T., and McDonough, M., 2001, "Experimental and Computational Investigation of Flow in Gas Turbine Blade Cooling Passages." 31st AIAA Fluid Dynamics Conf. and Exhibit, June 11-14, Anaheim, CA.

[8] Tsai, W.B., Lin, W.W., and Chieng, C.C., 2000, "Computation of Enhanced Turbulent Heat Transfer in a Channel with Periodic Ribs." Int. J. Nummerical Methods for Heat & Fluid Flow, Vol. 10, No. 1, pp. 47-66.

[9] Bredberg, J., and Davidson, L., 1999, "Prediction of Flow and Heat Transfer in a Stationary Two-Dimensional Rib Roughened Passage Using Low-Re Turbulent Models." Third European Conf. On Turbomachinery, IMECH C557/074/99.

[10] Kim, K.Y., and Kim, S.S., 2001, "Numerical Optimization of Rib Shape to Enhance Turbulent Heat Transfer. "Proceedings of the 2nd Int. Conf. On Computational Heat and Mass Transfer, COPPE/UFRJ – Federal University of Rio de Janeiro, Brazil, Oct. 22-26.

[11] Bredberg, J., Davidson, L., and Iacovides, H., 2000, "Comparison of Near-Wall Behavior and its Effect on Heat Transfer for k-ω and k-ε Turbulence Models in Rib-Roughened 2D Channels," 3rd Int. Symposium on Turbulence Heat and Mass Transfer, pp. 381-388.

[12] Morad, K., 2002, "The Manipulated Laminar Separated and Reattaching Flow: Investigation of Fluid Dynamic and Heat Transfer Enhancement." Port Said Engineering Journal, Faculty of Engineering, Suez Canal University, Vol. 6, No. 1, pp. 31-46.

[13] Kline, S.J., and McClintock, F.A., 1953, "Describing Uncertainties in Single-Sample Experiment," ASME J. Mechanical Engineering, Vol. 75, No. 1, pp 3-8.

[14] Kays, W.M., and Crawford, M.E., 1993, "Convective Heat and Mass Transfer, 3rd ed. McGraw-Hill, New York.

[15] Press, W.H., Flannery, B.P., Teukolsky S.A., and Vetterling, W.T., 1988."Numerical Recipes. "Cambridge University PRESS, New York.